# BES Analysis Memo
# Observation of $\psi(2S) \to \gamma\pi^+\pi^-$


Li Xinhua

*email: LIXH@bepc5.ihep.ac.cn*


(February 24, 1998)

## Abstract


A sample of $3.7 \times 10^6$ produced $\psi(2S)$ events collected by BES detector at BEPC is used to investigate the $\gamma\pi^+\pi^-$ decays. Significant production of $f_2$ has been observed which followes the expectation of the "15% *rule*".


The $\psi(2S)$ decay is conventionally compared with the corresponding $J/\psi$ decay to understand the nature of $c\bar{c}$ annihilation. In lowest order of perturbative QCD[1], the partial width of the $J/\psi$ or $\psi(2S)$ to three gluons is proportional to the square of the wavefunction at the origin, so is the partial width to leptons. If the hadronization of the gluons is not substantially different at the mass of $\psi(2S)$ from at the mass of $J/\psi$, one obtains a universal ratio

$$\frac{B(\psi(2S) \to X)}{B(J/\psi \to X)} = \frac{B(\psi(2S) \to ggg)}{B(J/\psi \to ggg)} = \frac{B(\psi(2S) \to e^+e^-)}{B(J/\psi \to e^+e^-)} = 0.146 \pm 0.022.$$

where X is an arbitrary non-charmonium state and the PDG[2] data are adopted for lepton pair decay.

Mark II collaboration has systematically investigated hadronic decays of $\psi(2S)$ and found most channels observe the theoretical expectation with absence of vector-pseudoscalar combinations, $\rho\pi$ and $K^*K$[3]. Over years, theoretic attempts have been taken without compelling explanation for the discrepancy between the ratios measured for the decays and theoretical expectation. Recently BES collaboration has observed that the hadronic decay of $\psi(2S)$ into vector-tensor combinations, $\omega f_2$, $\rho a_2$, $K^{*0}K_2^{*0}$, $\phi f_2'$, are suppressed at a level more than 3 [4].

The status of radiative decay is not clear because only a few of large upper limits is in PDG [2] for the non-charmonium decay of $\psi(2S)$. The lowest order expression of the partial width of $J/\psi$ or $\psi(2S)$ decay to a photon and two gluons also depends on the square of the wavefunction at the origin[5]. Thus one expects the "15% *rule*" stands also for radiative decays of $\psi(2S)$ and $J/\psi$ to any non-charmonium hadron. This memo dedicts to investigate the radiative decay of $\psi(2S) \to \gamma\pi^+\pi^-$. Specifically, we measure the branching fraction of $\psi(2S) \to \gamma f_2$.

The BES detector has been detailed in [6]. Here we briefly describle detector elements crucial to this measurement. Tracking is provided by a 10 superlayer main drift chamber (MDC). Each superlayer contains four layers of sense wires measuring both the position and the ionization energy loss ($dE/dx$) of charged particles. The momentum resolution is $\sigma_P/P = 1.7\%\sqrt{1+P^2}$, where P is the momentum in GeV/c. The resolution of $dE/dx$ measurement is about 9% for hadron tracks. This provides good $\pi/K$ separation and proton identification in low momentum region. An array of 48 scintillation counters surround MDC which measures the time-of-flight (TOF) of charged tracks with a resolution of 450 ps for hadrons. Outside the TOF system is an electromagnetic calorimeter composed of streamer tubes and lead blocks with a z positional resolution of 4 cm. The energy resolution scales as $\sigma_E/E = 0.22/\sqrt{E}$, where E is the energy in GeV. Surrounding the shower counter is a solenoidal magnet providing a 0.4 Tesla magnetic field in the central tracking region of the detector. The muon detector system lies outside the magnetic field and is used to measure the coordinates of muons in z and in $r\phi$ with resolution 5 cm and 3 cm, respectively. The analysis is based on a sample of $3.7 \times 10^6$ produced $\psi(2S)$ events collected by the Beijing Spectrometer detector at the Beijing Electron Positron Collider in the running from 1993 to 1995.

Events of two opposite charged tracks (MFIT=2) in the polar angle region $-0.8 < \cos\theta < 0.8$ have been selected. The cuts, $V_{xy} < 1.5cm$, $-15 < V_z < 15cm$ for each track, and $-5 < V_{z1} - V_{z2} < 5cm$ for two tracks combined, are attempted for event vertex to be in the colliding zone. Magnetic field correction is made to the momentum of charged track. Momentum corrections are further made for energy loss and multiple Coulomb scattering in the material before charged particles enter the drift volume in BES inner detector. So are photon directions entering shower counter for beam position dispersion in the colliding zone. Moreover, at least one neutral track with polar angle $-0.75 < \cos\theta < 0.75$ but outside the central ribbon range ($Z_{sc} < -4cm$ or $Z_{sc} > 4cm$) is selected for photon candidate. The angle between photon and charged track is also required to be larger than $30^o$.

Yuan Changzheng reported a check on the reliability of kinematic fit with BESLIB package TELESIS [7]. Using sample of $\psi' \to \pi^+\pi^- J/\psi$ where $J/\psi \to \mu^+\mu^-$, he found 14% difference between data and Monte Carlo if one cuts at confidence level of kinematic fit $> 0.01$. In another channel $e^+e^- \to \gamma\gamma$, he found 9% difference between data and Monte Carlo if the same cut is used. These significant differences may be due to the inappropriate error matrix of charge or neutral track which is used by kinematic fit to calculate the minimum $\chi^2$ of the fit. An investigation into the error matrix of charge track was detailed in [8]. An approach suggested by Bill Dunwoodie in June of 1997 was applied to test error matrix. The computed invariant mass error of resonance using the reconstructed error matrix which is stored in TRKLST is only 56% of the mass resolution observed on the mass spectrum in the channel $\psi' \to \pi^+\pi^- J/\psi$ where $J/\psi \to \mu^+\mu^-$. TELESIS package makes a particle species dependent correction for multiple Coulomb scattering (MCS) in beam pipe, gas and wire to error matrix of charged track. The mass error computed using the MCS corrected error matrix is only about 70% of the mass resolution observed on the mass spectrum in the same channel. The corresponding pull distributions of track quantities used in Kinematic fit give $\sigma > 1$ which also indicate the error matrix is too small. The error matrix is further scaled by $\sigma$ of pull distributions in order to make them close to 1 in further kinematic fit. The mass error computed using this further corrected error matrix can be very close to the mass resolution observed on the mass spectrum. The difference between data and Monte Carlo can then be decreased to 5% or less if one cuts at confidence level of kinematic fit $> 0.01$.

The error matrix are scaled by $\sigma$ of pull quantities for both charged and neutral track. For the simulated events of $\psi' \to \gamma f_2 \to \gamma\pi^+\pi^-$, Fig. 1 shows the pull distributions of kinematic fit before this correction. Fig. 2 is the corresponding confidence level. Fig. 3 is the same distribution after this correction. Fig. 4 shows the corresponding pull distributions. Fig. 5 is the pull distribution for the data where the above correction has been made to error matrix. Fig. 6 is the corresponding confidence level of kinematic fit. The latter two figures are made after all selections in this analysis note for the events with $\pi^+\pi^-$ mass in a region $0.5 - -2.0\ GeV/c^2$.

Events are kinematically $\gamma\pi^+\pi^-$ fitted and the corresponding confidence level is required to be greater than 0.01. The $dE/dx$ measurements are used to select pion tracks with confidence level larger than 0.003 for each track and 0.01 for all tracks combined. $R = E_{sc}/P$ is defined in order to remove electron. Any track with $P > 1GeV/c$ and $R > 1$ is removed as electron; Any pair of positive and negative tracks with both track $P > 1GeV/c$ and $(R_+ - 1)^2 + (R_- - 1)^2 < 0.36$ are removed. In order to remove $\mu$, $D^2 = (x_{proj} - x_{hit})^2 + (y_{proj} - y_{hit})^2$ is defined. $D < 4cm$ is taken as 1st layer $\mu$ counter hit, $D < 5cm$ as 2nd layer $\mu$ counter hit, and $D < 6cm$ as 3rd layer $\mu$ counter hit. Any pair of positive and negative tracks with (0,3), (1,2), (2,2), (2,3) or (3,3) $\mu$ counter hits are removed as muons. Events are also $\gamma k^+k^-$ fitted and $CL(\gamma k^+k^-) < CL(\gamma\pi^+\pi^-)$ is asked for. Extra photons hitting barrel shower counter with energy greater than 60MeV and angle to charged tracks larger than $16^o$ are investigated in Fig. 7 for data. Table 1 lists the selections to data and the simulation of $\psi(2S) \to \gamma f_2 \to \gamma\pi^+\pi^-$ and radiative Bhabha events. Fig. 8 - 12 show the $m(\pi^+\pi^-)$ plots rejected by the above selections to data.

Fig. 13 is the $\pi^+\pi^-$ mass spectrum in high mass region ($m > 2.9GeV/c^2$) for the surviving events. Fig. 14 is the corresponding plot in low mass region ($m < 2.9GeV/c^2$) which indicates the production of $f_2$ and also a lower mass structure around $\rho^0$ which consists with a QED process - initial state radiation of photon by the $e^+$ or $e^-$, followed by $e^+e^- \to$ vector meson [9]. It is unbinned fitted to two Breit-Wigner curves with the corresponding width fixed to PDG added to a quadratic background (Fig. 15). The mass resolution is 7.6MeV for $f_2$, and 5.7MeV for $\rho^0$, respectively. The combined fit leads to $130.8 \pm 27.6$ $f_2$ signal with mass $(1242.1 \pm 16.7)MeV$, and $192.6 \pm 23.7$ $\rho^0$ signal with mass $(740.2 \pm 9.0)MeV$. The corresponding fit plot to Monte Carlo is shown in Fig. 16 for comparison.

Several checks have been performed to the $\pi^+\pi^-$ mass structure. Radiative Bhabha events have been checked with 5000 events generated in the polar angle region $|\cos\theta| < 0.85$. Fig. 18 shows the $\pi^+\pi^-$ mass for the selected events where contamination into low mass region ($m < 2GeV/c^2$) is not significant. The $\tau$ scanning data taken in 1991 at BEPC have also been analyzed in the similar way where the data of 12 energy points are combined because of small energy intervals. The resulting $\pi^+\pi^-$ mass plot (Fig. 17) indicates also a $\rho^0$ structure with the $f_2$ resonance absent. The $\pi^+\pi^-$ mass spectrum has also been looked in the decay $J/\psi \to \gamma\pi^+\pi^-$ via the process of $\psi(2S) \to \pi^+\pi^- J/\psi$. The resulting $\pi^+\pi^-$ mass plot (Fig. 19) indicates the similar structure to Fig.15 in low mass region ($m < 2GeV/c^2$). The mass structure around $\rho^0$ is a contamination of $\psi(2S) \to \pi^+\pi^- J/\psi$ with $J/\psi \to \rho^0\pi^0$ which is shown on Fig. 20 of a simulation. An unbinned fit to figure 19 with two Breit-Wigner curves ($\rho^0$, $f_2$) and background in mass region $0.2 - -2.5$ GeV presents the following: $\chi^2 = 20.88/20$ dof; $\rho^0$ mass=$790.3 \pm 4.6$ MeV, width=$147.7 \pm 15.1$ MeV, and events $560.3 \pm 43.5$; $f_2$ mass=$1258.6 \pm 10.6$MeV, width=$155.85 \pm 31$ MeV, and events $225.5 \pm 32.8$. Mass resolution is fixed to 7.6MeV for $f_2$ and 5.7 MeV for $\rho^0$ in the fit. Analysis efficiency of $\psi' \to \pi^+\pi^- J/\psi$ with $J/\psi \to \gamma f_2$ is 0.188 where 15000 events are produced with $\psi'$ generator of $\psi' \to \pi^+\pi^- J/\psi$ and uniform phase space of $J/\psi \to \gamma f_2$.

$$B(J/\psi \to \gamma f_2) = (1.76 \pm 0.26) \times 10^{-3}$$

is computed with only error of fitted event number. It is compatible with the PDG values

$$B(J/\psi \to \gamma f_2) = (1.38 \pm 0.14) \times 10^{-3}$$

The $\rho^0$ mass in $J/\psi \to \gamma\pi^+\pi^-$ in the process $\psi' \to \pi^+\pi^- J/\psi$ is higher than that in PDG. It's actually from a contamination of $J/\psi \to \rho^0\pi^0$. A check is applied to Monte Carlo. Events of $\psi' \to \pi^+\pi^- J/\psi$ with $J/\psi \to \rho\pi$ using $\psi'$ generator are produced. Using unbinned Breit-Wigner fit to the $\pi^+\pi^-$ mass analyzed in $\psi' \to \pi^+\pi^- J/\psi$ with $J/\psi \to \gamma\pi^+\pi^-$, I got $\rho^0$ mass higher than PDG value ($768.5 \pm 0.6$ MeV): $788.2 \pm 6.8$ MeV when its width is free in the fit (the fitted value is $113.9 \pm 18.7$ MeV), and $789.3 \pm 7.5$ MeV when the width is fixed to PDG value 150.7 MeV in the fit.

The analysis efficiency of $\gamma f_2$ is 39.2% calculated by Monte Carlo simulation with uniform phase space distribution and combining detector status in addition to data process. Adopting an isospin ratio 2:1 for $f_2$ decays into $\pi^+\pi^-$ and $\pi^0\pi^0$, one obtains

$$B(\psi(2S) \to \gamma f_2) = (1.59 \pm 0.34 \pm 0.41) \times 10^{-4}$$

where the first error is statistic, and second systematic which results from event selection (18%), $\psi(2S)$ event number (10%), branching fraction of $f_2 \to \pi^+\pi^-$ (2.9%), and simulated efficiency (15%). A comparision of $\psi(2S)$ decay to $J/\psi$ is processed by using the branching fraction of $B(J/\psi \to \gamma f_2) = (1.38 \pm 0.14) \times 10^{-3}$ in PDG [2]. One observes

$$\frac{B(\psi(2S) \to \gamma f_2)}{B(J/\psi \to \gamma f_2)} = (11.5 \pm 4.0)\%$$

which indicates that the radiative channel $\gamma f_2$ obeys the "15% *rule*" in the $\psi(2S)$ and $J/\psi$ decay.

In summary, we observed the $f_2$ production in radiative decay of $\psi(2S)$ in $3.7 \times 10^6$ data sample and even an initial state radiation production of $\rho^0$. The decay of $\psi(2S)$ to $\gamma f_2$ is compared with the corresponding $J/\psi$ decay and consistent with perturbative QCD expectation.

# REFERENCES

[1] T.Applequist, D.Politzer, Phys. Rev. Lett. 34, 43(1975).
[2] Particle Data Group, Phys. Rev., D54, 1(1996).
[3] M.E.B.Franklin et al., Phys. Rev. Lett. 51, 11(1983).
[4] BES Collaboration, to be submitted to Phys. Rev.
[5] W. Kwong, Phys. Rev., D37 (1988) 3210.
[6] BES Collab., Nucl. Instr. Methods, A344 (1994) 319.
[7] Yuan Changzheng, Talk at BES Monthly Meeting on Dec. 5, 1997.
[8] Li Xinhua, Talk at BES Monthly Meeting on Dec. 5, 1997.
[9] J.D. Jackson and D.L. Scharre, Nucl. Instr. Methods, 128, 13(1975); G.Bonneau and F.Martin, Nucl. Phys. B, 27, 381(1971).

Table 1. A tabulation of the $\gamma\pi^+\pi^-$ selections

| | data | simulated $\gamma f_2$ | simulated $\gamma e^+e^-$ |
|---|---|---|---|
| Generated | | 11100 | 5000 |
| Nchrg=2, $\mid \cos\theta \mid < 0.8$ | 2196995 | 6441 | 3318 |
| Vertex | 1254387 | 6351 | 3307 |
| Photon | 378308 | 5847 | 112 |
| pass 4C | 36588 | 4978 | 65 |
| $CL(4C) > 0.01$ | 22199 | 4758 | 58 |
| $CL(dE/dx) > 0.01$ | 6222 | 4726 | 58 |
| Reject electrons | 6074 | 4726 | 13 |
| Remove muons | 4226 | 4637 | 13 |
| $CL(\gamma\pi^+\pi^-) > CL(\gamma k^+k^-)$ | 2761 | 4465 | 10 |

## FIGURES

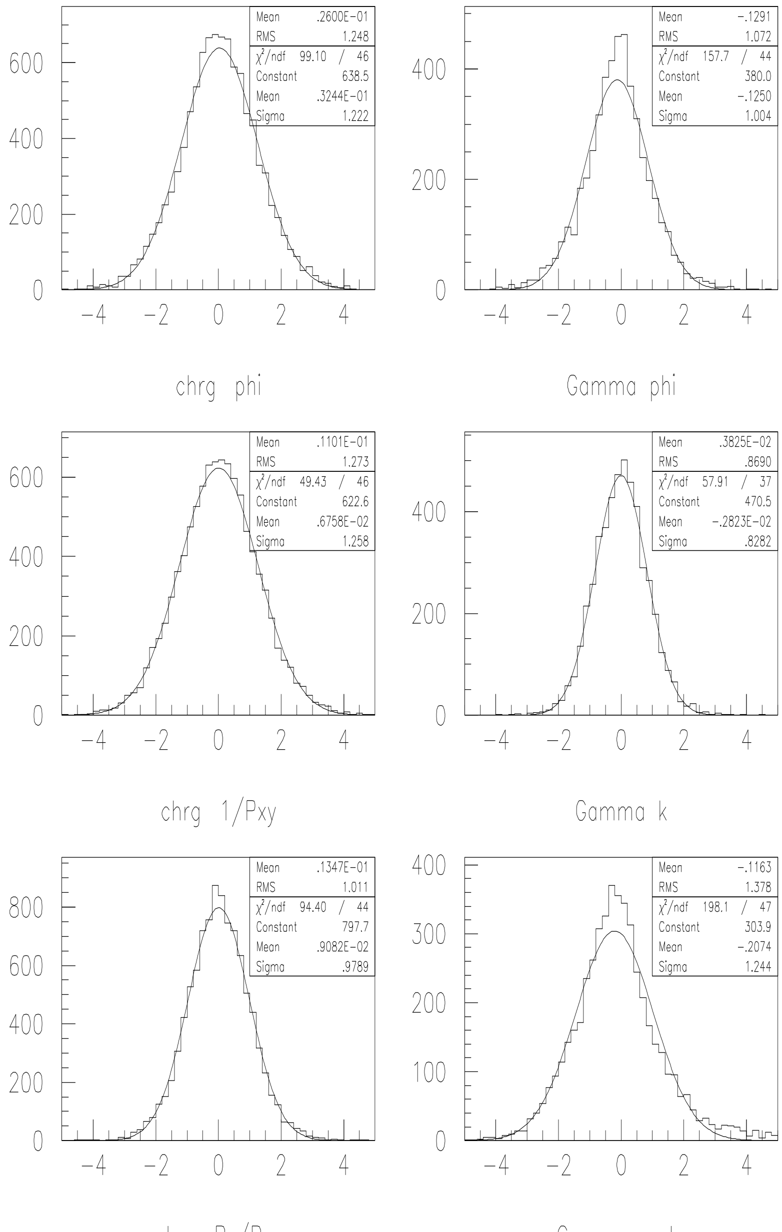


FIG. 1. Pull distribution of kinematic fit before error matrix scaling in Monte Carlo $\psi(2S) \to \gamma f_2$

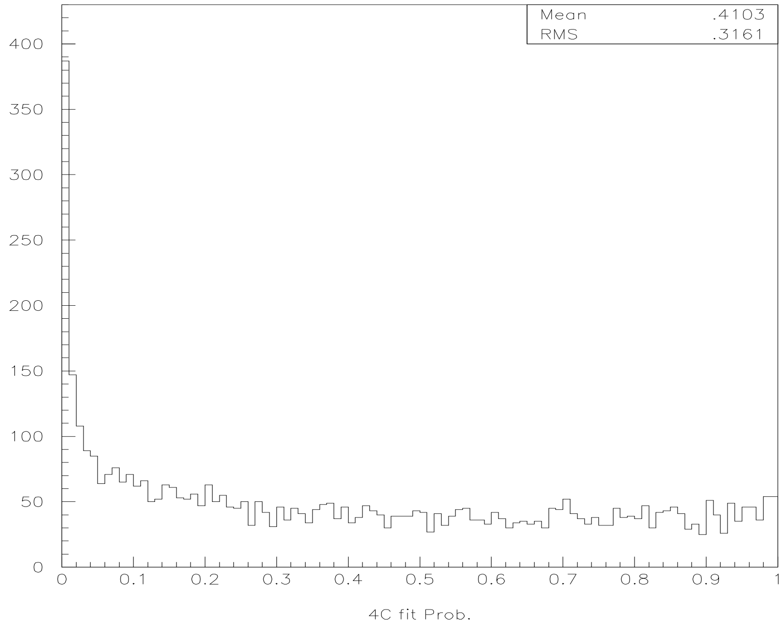


FIG. 2. Confidence level of kinematic fit before error matrix scaling in Monte Carlo $\psi(2S) \to \gamma f_2$

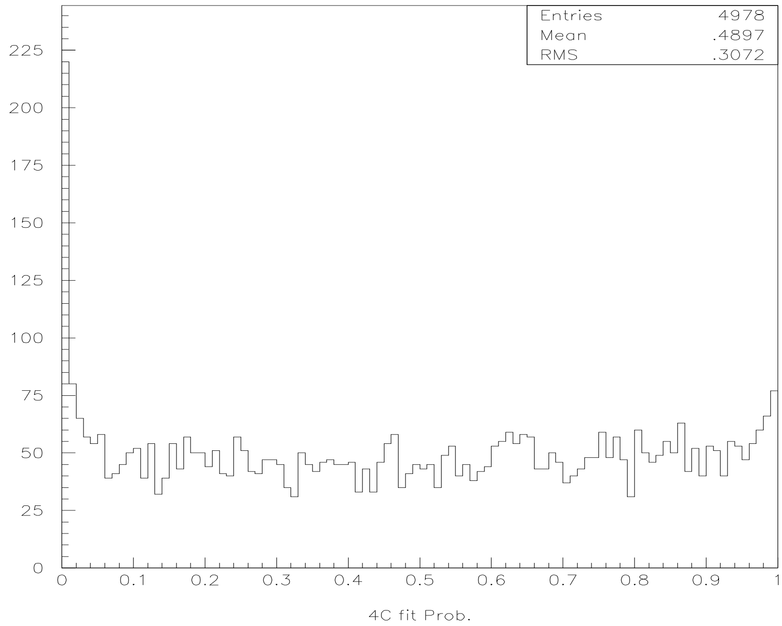


FIG. 3. Confidence level of kinematic fit after error matrix scaling in Monte Carlo $\psi(2S) \to \gamma f_2$

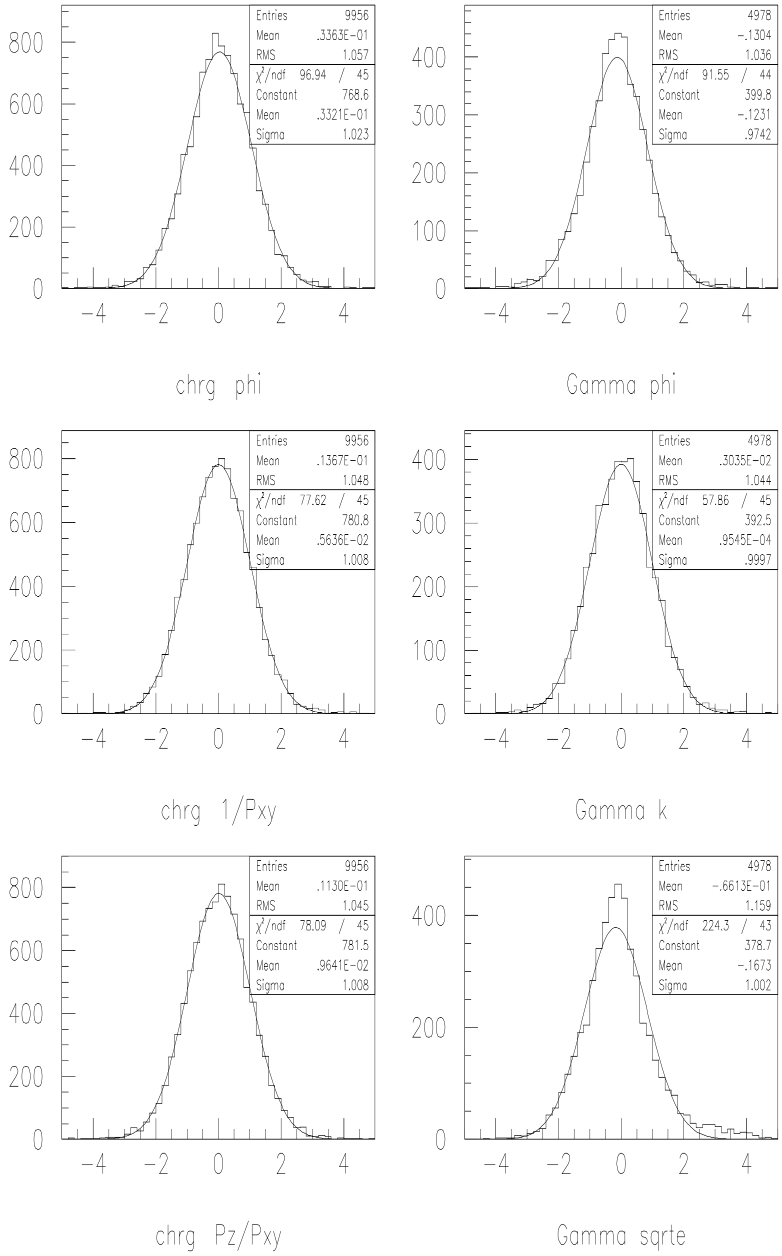


FIG. 4. Pull distribution of kinematic fit after error matrix scaling in Monte Carlo $\psi(2S) \rightarrow \gamma f_2$

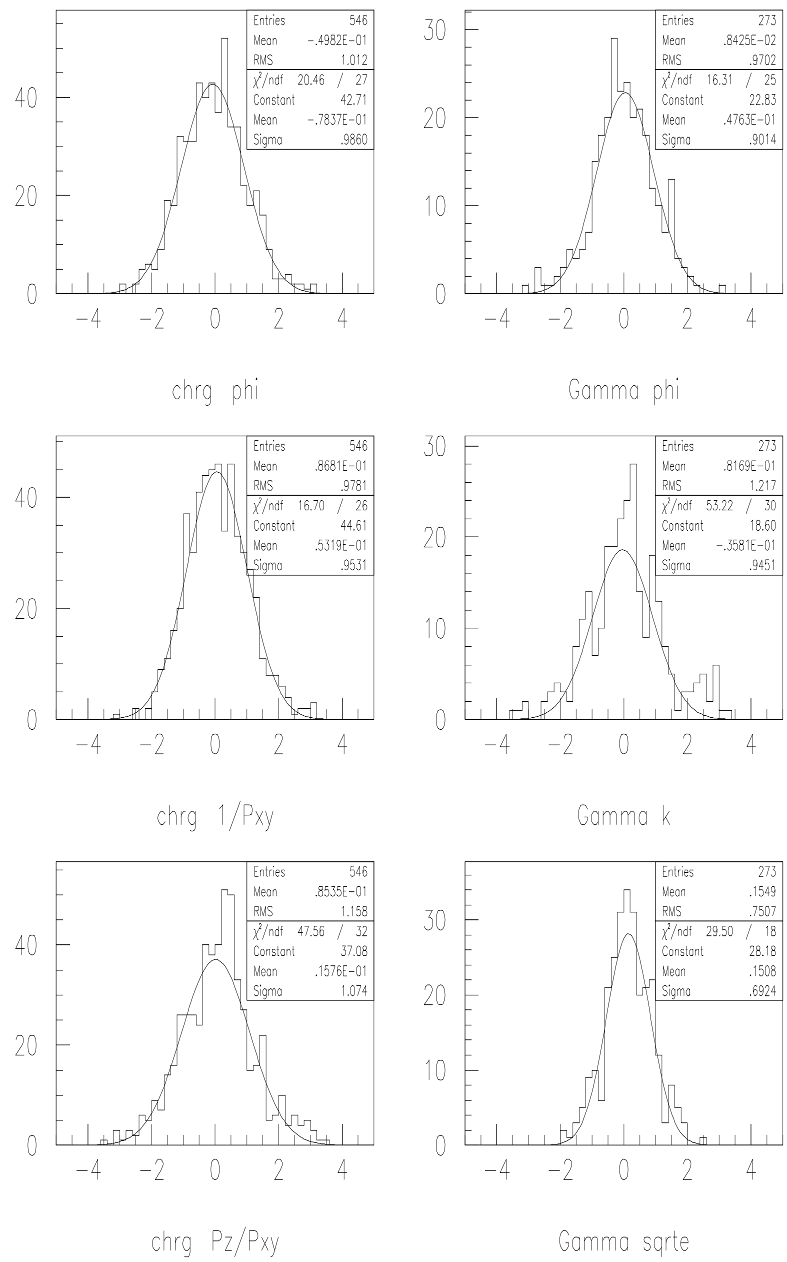


FIG. 5. Pull distribution of kinematic fit after error matrix scaling and all selections for events $0.5 < m(\pi^+\pi^-) < 2$ GeV in data

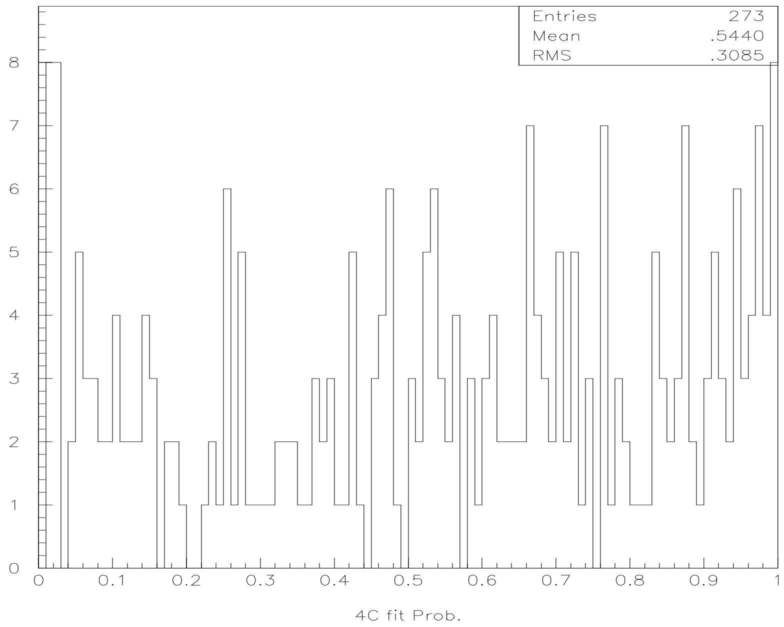


FIG. 6. Confidence level of kinematic fit after error matrix scaling and all selections for events $0.5 < m(\pi^+\pi^-) < 2$ GeV in data

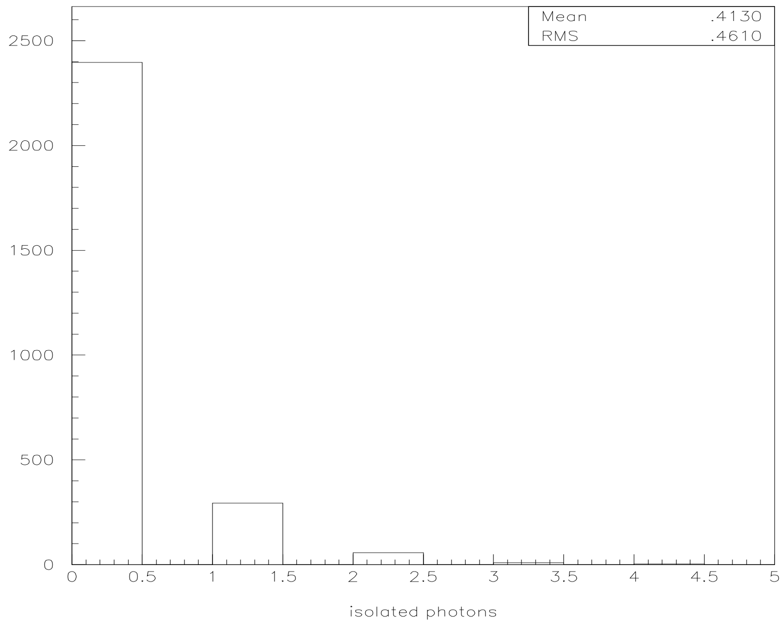


FIG. 7. Extra photons in the selected $\gamma\pi^+\pi^-$ events

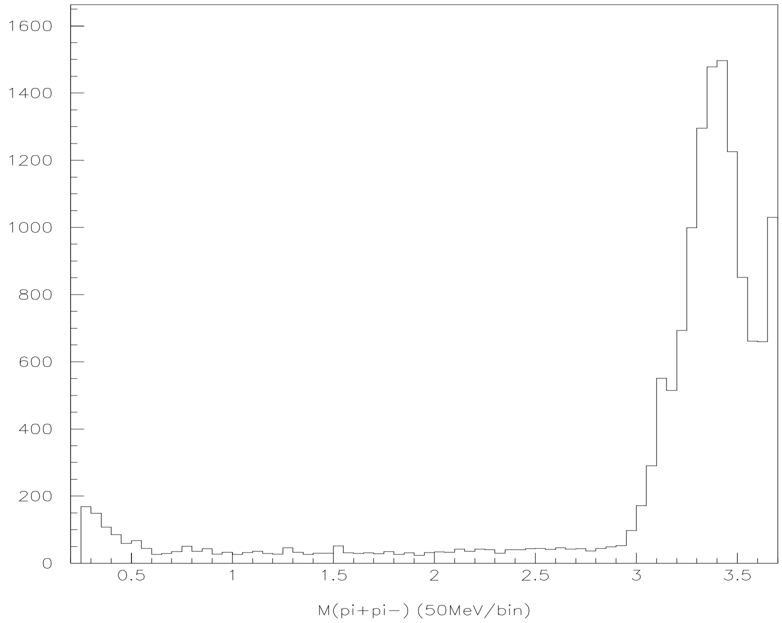


FIG. 8. $M(\pi^+\pi^-)$ plot of the events rejected by the selection of $CL(4C) > 0.01$

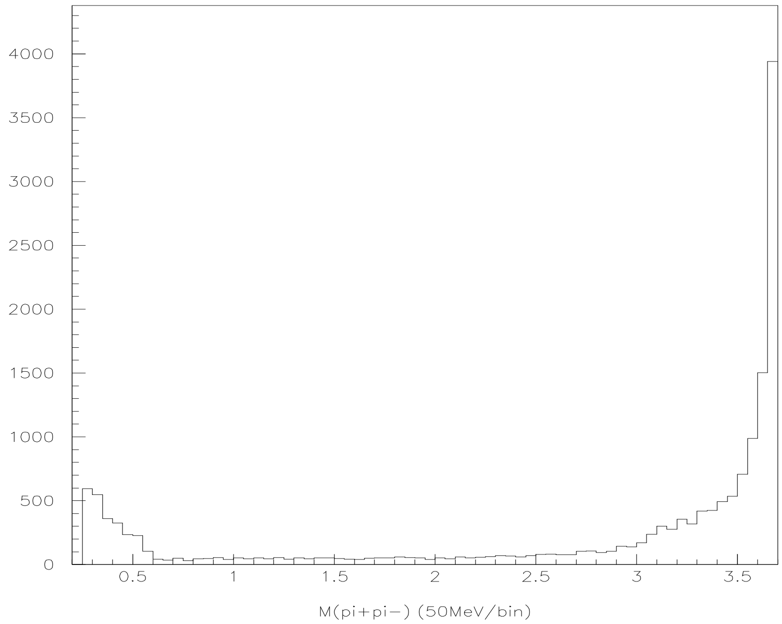


FIG. 9. $M(\pi^+\pi^-)$ plot of the events rejected by dE/dx selection

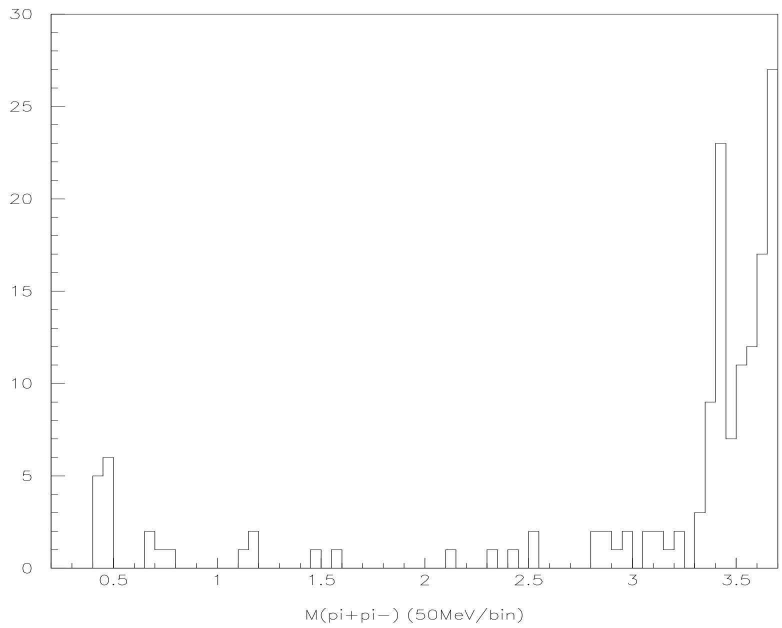


FIG. 10. $M(\pi^+\pi^-)$ plot of the events rejected as electrons

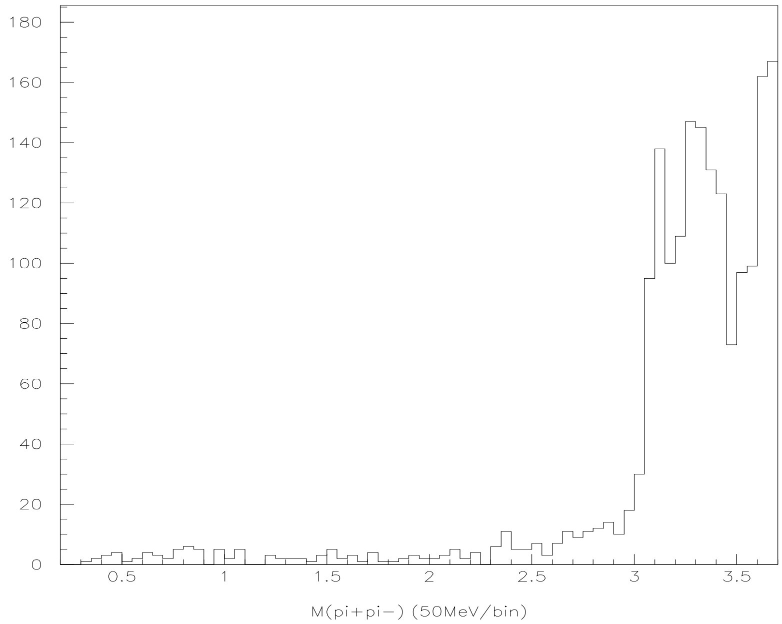


FIG. 11. $M(\pi^+\pi^-)$ plot of the events rejected as muons

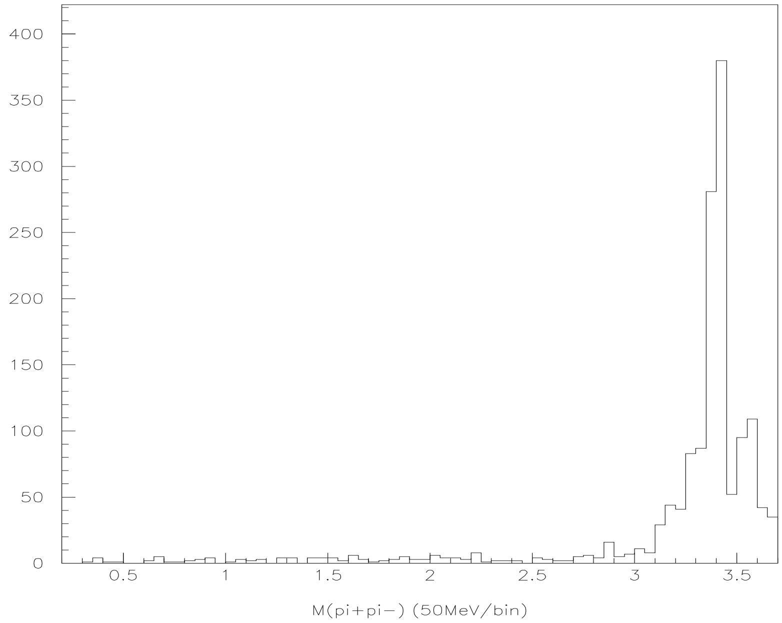


FIG. 12. $M(\pi^+\pi^-)$ plot of events rejected by $CL(\gamma\pi^+\pi^-) < CL(\gamma K^+K^-)$ in kinematic fit

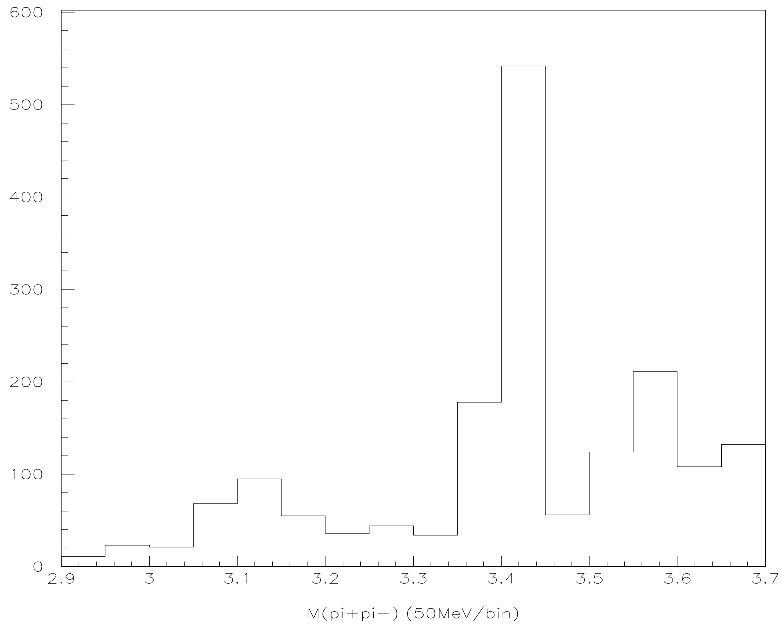


FIG. 13. $M(\pi^+\pi^-)$ plot of the selected events in high mass region.

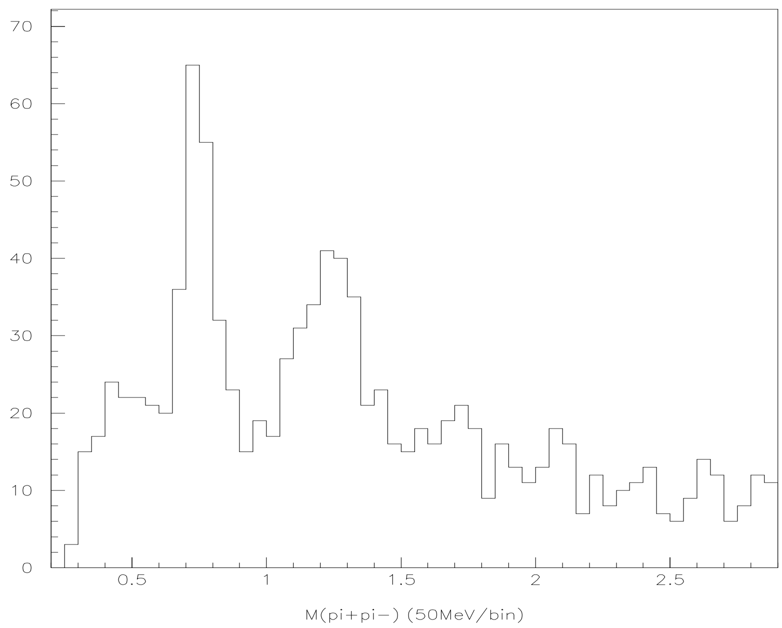


FIG. 14. $M(\pi^+\pi^-)$ plot of the selected events in low mass region.

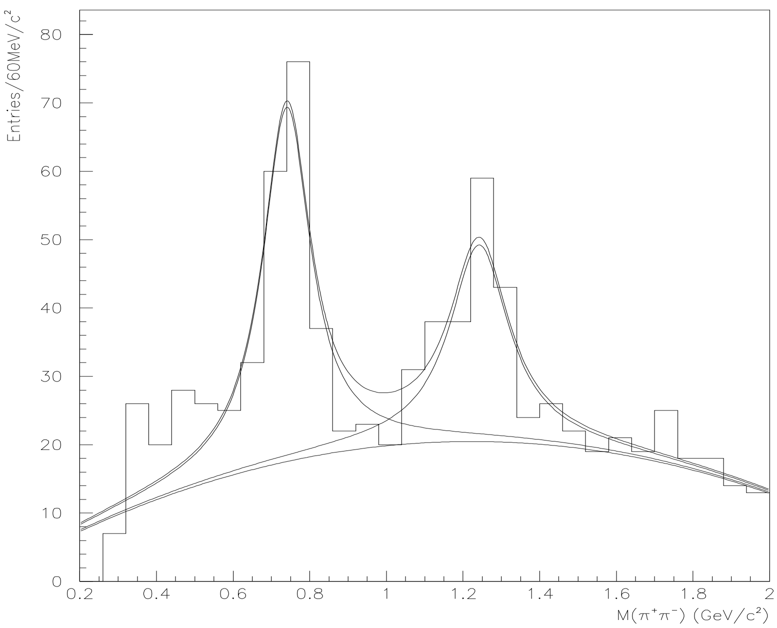


FIG. 15. Fit to $M(\pi^+\pi^-)$ spectrum in data.

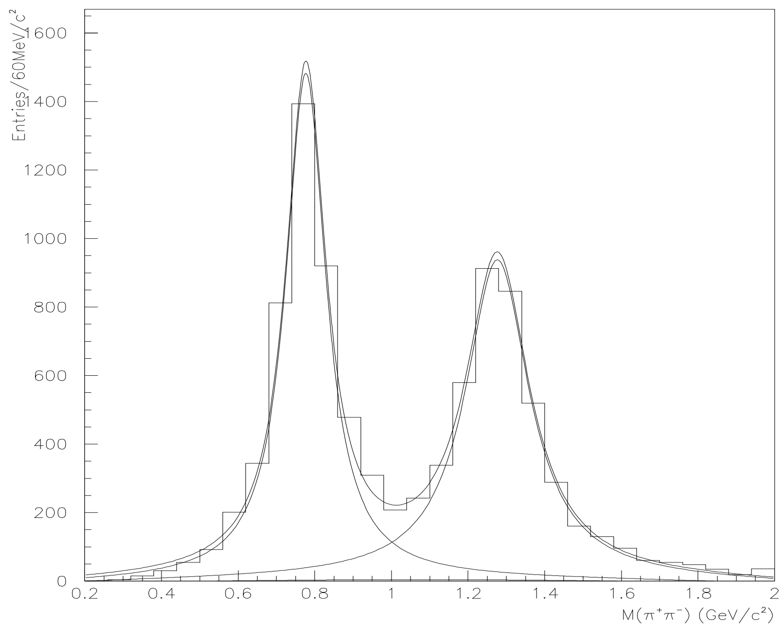


FIG. 16. Fit to $M(\pi^+\pi^-)$ spectrum in Monte Carlo $\psi(2S) \to \gamma f_2$.

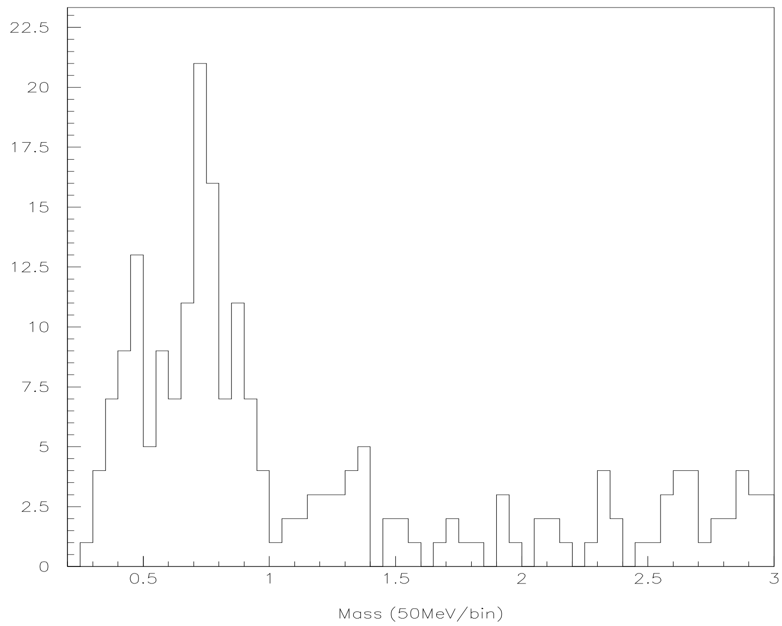


FIG. 17. $M(\pi^+\pi^-)$ spectrum in $\tau$ scanning data where $\rho^0$ is produced in initial state radiation.

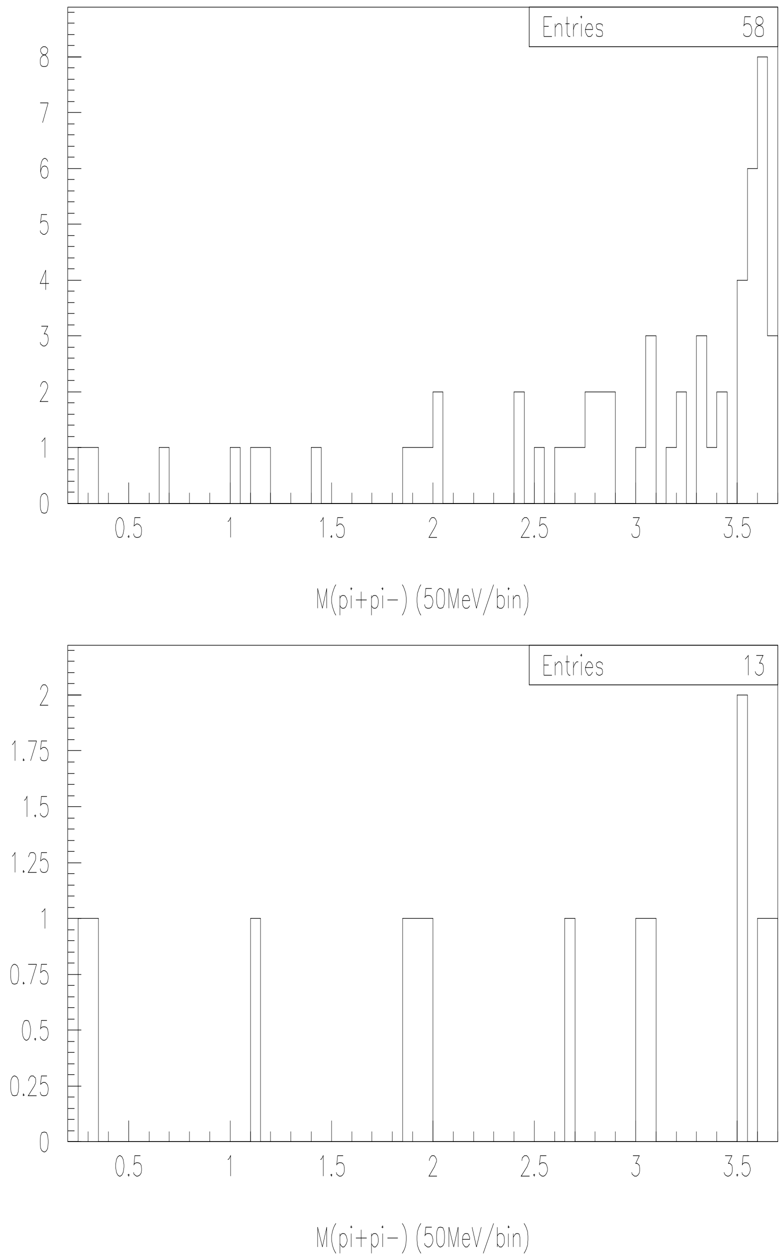


FIG. 18. $M(\pi^+\pi^-)$ spectrum in the simulation of Bhabha events: upper plot: after dE/dx selection $CL(dE/dx) > 0.01$; lower plot: after $\mu$ rejection.

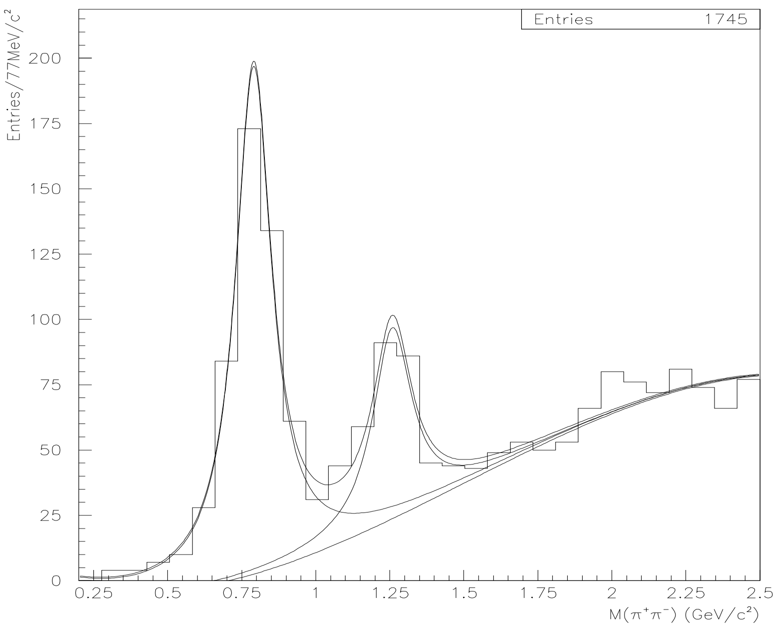


FIG. 19. $m(\pi^+\pi^-)$ spectrum in the decay $J/\psi \to \gamma\pi^+\pi^-$ via the process of $\psi(2S) \to \pi^+\pi^- J/\psi$.

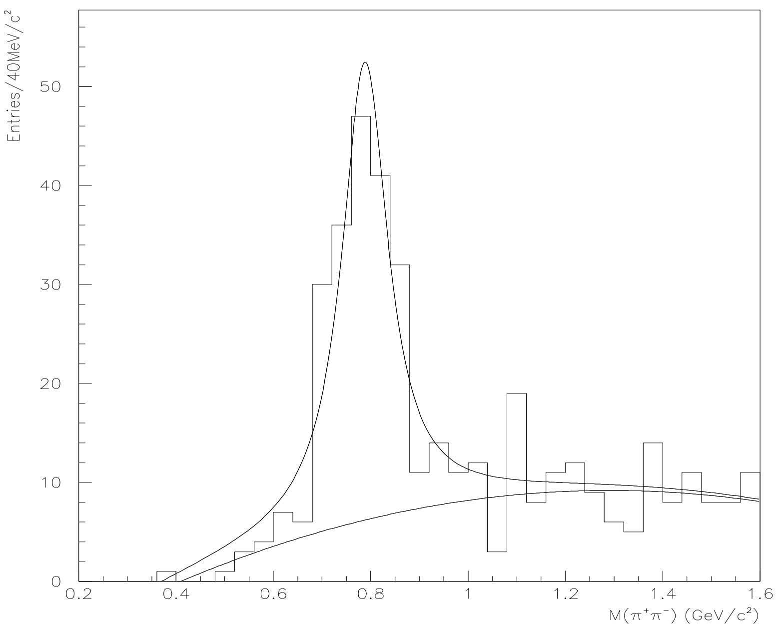


FIG. 20. $m(\pi^+\pi^-)$ spectrum in the simulation of $\psi(2S) \to \pi^+\pi^- J/\psi$ with $J/\psi \to \rho\pi$.